Operator related attenuation effects in radiometric surveys

E. Buchanan[1†], A.J. Cresswell[2,*], B. Seitz[1], D.C.W. Sanderson[2]

[1] SUPA School of Physics and Astronomy, University of Glasgow, UK

[2] Scottish Universities Environmental Research Centre, East Kilbride, UK

[*]Corresponding Author: email: alan.cresswell@glasgow.ac.uk, tel: +44 (0)1355 270107, fax: +44 (0)1355 229898

[†]Present address: School of Physics, University of Bristol, UK

Abstract

Radiometric surveys using airborne, vehicular mounted or backpack detector systems are increasingly used to identify and evaluate complex distributions of radioactivity in the environment. The signals detected depend on the energy and spatial distribution of radioactive sources, the material properties of the environment and the specific properties of the detector systems employed. Materials in close vicinity to the detector such as housings, and intermediate materials may have a critical impact on detection efficiency, and must therefore be taken into account in calibration. This study evaluates the effect of shielding by the body of the operator in backpack surveys. Controlled experiments using point sources and absorbers, chosen to represent the form and composition of human tissue, were conducted, and coupled to an analytical radiation transport model to estimate attenuation factors for mapping of ^{137}Cs. In this way generic factors to correct for this effect using portable spectrometers have been determined. The results compare well with observations at sampled calibration sites in Fukushima and the Solway area in Scotland. Reductions of the ^{137}Cs full-energy peak intensity between 20% and 30% may be expected depending on operator stature and the offset position of backpack systems. Similar effects may be present for other radiometric systems carried by a human operator.

Keywords: Environmental radioactivity, gamma ray survey, attenuation by human operator

Highlights:

- Evaluation of operator effects on radiometric measurements with backpack systems
- Potential for similar effects with other radiometric systems
- Count rates for radiocaesium full energy peaks are reduced by 20-30%
- Count rates for >450 keV, scaling to dose rate, are reduced by approximately 15%

1. Introduction

Radiometric surveying measures the spatial distribution of radiation in the environment. The aim of a radiometric survey is to evaluate the distribution of radioisotopes in the environment, taking natural and artificial passive materials affecting the radiation field at any given point into account. Applications of this method are wide ranging, including nuclear site baseline surveys (Sanderson *et.al.* 1990a, 1992a, b, 1994c,d, Bucher *et.al.* 2008), mapping fallout from nuclear accidents (Mellander 1989, Sanderson & Scott 1989, Sanderson *et.al.* 1989, 1990b, 1993a, 1994a, Drovnikov *et.al.* 1997), remediation (Giles *et.al.* 2005), locating point sources (Aage & Korsbech 2003, Hjerpe & Samuelsson 2006, Long & Martin 2007, Kock *et.al.* 2014), geological mapping for mineral exploration (IAEA 1991, 2003, Minty 2011) or epidemiology (Sanderson *et.al.* 1993b), and environmental process monitoring (Sanderson *et.al.* 1994b, Tyler & Heal 2000). In the aftermath of the nuclear accidents at the Chernobyl and Fukushima Dai-ichi nuclear power plants such methods have gained wider attention and recognition (Sanderson & Ferguson 1997, Sanderson *et.al.* 2004, Winkelmann *et.al.* 2004, Lyons & Colton 2012, Sanderson *et.al.* 2013, Tanigaki et.al. 2013, Sanada et.al. 2014, Kobayashi et.al. 2015, Tsuda et.al. 2015).

The spectrometry systems used for these surveys usually consist of scintillation crystal or HPGe detectors, singularly or in arrays, with a spectrometer, a GPS receiver that registers the position of each measurement and a mobile computer to collect and analyse the data. The spectrometer systems can be mounted on either low flying aircraft, ground based vehicles or

backpacks that are carried by human operators. Each method has different benefits and drawbacks. Aircraft flying at low altitudes offer large fields of view and the highest rates of area coverage (10^7-10^8 m^2 hr^{-1}) but with spatial resolution limited to 50-100 m dimensions, and need to address issues relating to operational safety and potential nuisance over urban environments. Vehicles allow relatively rapid surveys of roads and some off-road locations, but are restricted by terrain, and influenced by local shielding effects. Backpack detectors have relatively low rates of area coverage, and with spectral sensitivity limited by small detectors normally used. These limitations however are considerably offset by the ability of backpack surveys to provide high resolution (1-10 m or better) analysis of environments where people live and work, which would otherwise be difficult to survey in detail, and where radiation fields both due to natural and anthropogenic activity are highly variable.

To interpret radiometric data and estimate the spatial activity distribution, the response of the detector system and the effects of the platform are required. The intrinsic efficiency and angular dependence of detector systems can be measured in the laboratory and relatively easily modelled. The effect of the measurement platform is potentially more complex, and must be taken into account in system calibration and in interpreting results. For airborne systems, detectors are usually placed with the minimum possible material beneath and around the detector. Some aircraft have fuel tanks located in positions which may impact radiation transport in a time-varying manner, and these should be avoided where possible. For vehicular systems it is common to place detectors in elevated positions, often on the vehicle roof, to maximize the field of view. In such cases, the detector field of view includes the complex structures of the vehicle and occupants, and often a fuel tank. For backpack systems, the operator carrying the system subtends a significant proportion of the detector field of view. These provide a complicated shaped radiation shield very close to the detector and with potential to distort spatial response characteristics, and to bias results if not taken into account by suitable calibration. An example of this effect is reported by Nilsson et.al. (2014), when a backpack survey of a test site containing radioactive sources produced irregular features caused by shielding of the detector when walking towards a source.

In this paper, the effect of the operator on radiometric data collected with backpack systems is investigated using a combination of numerical and experimental modelling and field observations. These effects have implications for the design of backpack systems and their calibration, may affect design of surveys especially in spatially complex environments where

the details of the spatial response of the detector may be significant. This study also has implications for other detector systems, including portable dose rate instruments, where similar effects may be present.

This study has been conducted using a portable gamma spectrometry system developed at the Scottish Universities Environmental Research Centre (SUERC). This consists of a 3x3" NaI(Tl) detector with digital spectrometer and GPS receiver in a waterproof container, with a tablet computer collecting data and providing outputs from real-time analysis. The system has been described elsewhere (Cresswell *et.al.* 2013), and has been used for a variety of radiometric survey tasks including mapping beaches potentially contaminated with radioactive particles (Cresswell & Sanderson 2012), mapping urban areas (Cresswell *et.al.* 2013) and mapping deposited activity from the Fukushima Daiichi accident (Sanderson *et.al.* 2013).

2. Method

Previous field measurements (Sanderson *et.al.* 2013, Cresswell *et.al.* 2013) indicate a significant reduction of spectral intensities when the backpack detector system is worn by a human operator compared to an isolated detector system, with corresponding shortfalls in estimated activity per unit area in comparison with soil samples of reference sites if theoretical calibration constants for the unshielded detector are used to determine sensitivity. One solution to this problem is to determine sensitivities by calibration measurements at well sampled reference sites. Here the systematic effects are examined further by a combination of numerical and experimental modelling, and comparison to field measurements. In this approach a simple shaped substitute operator was used in the experiment and compared to a numerical model of the same geometry. The studies concentrate on ^{137}Cs, as this is not only indicative of the mean gamma energy measured in many studies of NORM isotopes, but is also a prime indicator for anthropogenic releases e.g. in the aftermath of a nuclear incident. Using known and tabulated energy dependent attenuation coefficients the model is extendable to other energy ranges.

2.1 Radiation Transport for Numerical Modelling

The count rate observed at a detector is a function of the source activity A_s, geometrical acceptance and distribution of the source, detection efficiency ε and possible attenuation of the emitted radiation between the source location and the position of the detectors, expressed in a complex function *F(E)*, which is dependent on the energy *E* of the incident photon. For complex sources, the gamma ray emission probability γ has to be taken into account as well. In general, the detection efficiency ε will also be a function of the gamma ray energy, the incident position *x* on the detector surface and the direction of the gamma ray at the detector surface, $\varepsilon = \varepsilon\,(E_{gamma}, x, \theta, \varphi)$. Note, that this definition of the detection efficiency ε combines the geometrical and energy dependent efficiency factors into one common factor.

Let the detector have a surface area A_d at a distance P_{total} from an isotropic point source of given gamma energy E_{gamma}. For all dimension of the detector being much smaller than P_{total} and in the case of an isotropically emitting point source, the geometrical acceptance (or solid angle coverage) can be approximated as $A_d \Big/ 4\pi P_{total}^2$. With $P_{total} = \sum_i P_i$ and given linear attenuation coefficients $\mu_i(E_{gamma})$ the total attenuation of the gamma rays through *n* different materials is given as $F(E) = \sum_i e^{-\mu_i(E)P_i}$. The total gamma activity is given by γA_s. The observed count rate *R* is then:

$$R = \frac{A_d}{4\pi P_{total}^2}\gamma A_s \varepsilon\left(E_{gamma}, \theta, \varphi, x\right)F(E) \qquad \text{Eq. 1}$$

The attenuation in different materials factorises. It is therefore convenient to separate *F(E)* into materials external to the detector system, i.e. the path through soil, air, the body of the observer and other passive materials, and internal to the detector system, i.e. entrance windows, packaging etc. The external materials will be explicitly parameterised, while the internal effects will be subsumed in an effective efficiency ε, which is determined experimentally (section 2.3).

2.2 Human Form and Its Attenuation Properties

2.2.1 General Properties of the Human Body

The variability of mass shape and composition of individual operators is potentially large. So this work refers to the definitions given by the International Commission of Radiological

Protection (ICRP) reports 23 ("The Report on the Group Task on Reference Man") and 89 ("Basic Anatomical and Physiological Data for use in Radiological Protection: Reference Values") (ICRP 1975, 2002). These define physical parameters for reference adults, as summarised in Table 1. These reports also describe elemental compositions for organs in the human body, and in ICRP23, average compositions for an adult body.

The average elemental composition for the reference adult whole body, given in Table 2, was used to determine the average mass attenuation coefficient of a human operator, neglecting any details of the internal body structure. Tabulated elemental mass attenuation coefficients (Storm & Israel, 1970) were scaled to the body composition. Linear attenuation coefficients were determined assuming an average body density of 1060 kg m^{-3}. The mass and linear attenuation coefficients for 662 keV (^{137}Cs) were determined by a local fit between 100 keV and 1500 keV where, on a log-log plot, there is a simple relationship between attenuation coefficient and gamma ray energy. The attenuation coefficients determined are given in Table 3. Following this approach the gross features of the human body are replicated, while detailed anatomical structure is neglected.

2.2.2 Substitution Materials and Shapes for the Human Body

Because of the complexity of the shapes of the human body and the ethical considerations associated with conducting point source experiments with human operators, a simplified substitute was used for the numerical and experimental models. This substitute must have similar mass, linear attenuation, density and dimensions as the human body, while being easy to use and model reliably.

The attenuation coefficients for commonly available materials were calculated from tabulated elemental mass attenuation coefficients as before. These coefficients, with others used in the model here, are given in Table 4. Other tabulations of attenuation coefficients include similar materials, and values derived here were compared to those. The calculated values deviate by 1-3% from the National Institute of Standards and Technology (NIST, Hubble & Seltzer 2004) values.

Many body dummies used to study car crashes or employed in search and rescue training as well as medical testing phantoms are made from PVC and come in dimensions similar to the

"Reference Man". The linear attenuation and density of PVC at the relevant gamma energy (662 keV) are slightly larger than the average computed for the human body. In addition, these dummies and phantoms are often internally supported by complex metal structures with significantly higher attenuation coefficients, which are difficult to model accurately.

For the numerical model a simplified cuboid body shape of width 0.4 m, depth 0.3 m and height 1.7 m was considered, with linear attenuation coefficients for the average human body. For the experimental model this was reproduced using a stack of 0.30x0.40x0.23 m plastic boxes filled with water.

2.3 Detector Angular Response

The effective detection efficiency ε can be experimentally obtained from an observed count rate $\dot{C}$ using a calibrated source of known gamma activity γA_s at a distance r from a detector of surface area A_d

$$\varepsilon(662keV,\theta) = \frac{4\pi dr^2\dot{C}}{A_d\gamma A_s e^{-\mu_{air}r}} \qquad \text{Eq. 2}$$

Note that self-absorption in the source and backscattering are neglected and attenuation in the detector housing and angular dependence on A_d are subsumed in ε.

Measurements were conducted on an open laboratory bench using ^{137}Cs point sources totalling 440 kBq at a distance r=1.5 m from the centre of the detector crystal. The detector was rotated on the bench top in 15° steps, with spectra recorded for approximately 10 mins at each position and the count rate in a window around the ^{137}Cs peak recorded. Count rates for background spectra were subtracted. Measurements of the background at different rotational positions differed by less than 1%, and a mean value for the whole background data set was used. The net count rates for each position were substituted into equation 2, using A_d=$\pi 0.038^2$ m^2 corresponding to the area of the end of the detector crystal. The calculated efficiency is shown in Figure 1.

The angular response of the SUERC backpack system shows a small minimum around 0°, corresponding to attenuation by the GPS receiver, and a significant reduction in efficiency through the photomultiplier and digital spectrometer at 180°. The angular response of bare

cylindrical detectors has been described using a function of the form $a+b.cos\theta$ (Grasty 1979, ICRU 1994), giving a maximum efficiency at 90°. Such a function fails to account for the modification of the angular response observed for the backpack system, as it does not account for additional attenuation by the photomultiplier and digital spectrometer assembly, the GPS and the weatherproof container. Additional terms of the form $c.sin^2\theta$ and $d.cos^2(e\theta)$ were evaluated to fit the observed distributions. $c.sin^2\theta$ introduces a maximum at 90°, but still retains relatively high efficiency at 180°. $d.cos^2(e\theta)$, where e≈0.5, introduces an efficiency term that peaks at 0° with a minimum at ≈180°. A fit to a function of the form

$$\varepsilon = a + b\cos\theta + c\sin^2\theta + d\cos^2 e\theta$$

should therefore reproduce the observed distribution. Figure 1 shows such a fit. In this instance c was very close to zero, and the $c.sin^2\theta$ term has been omitted from the fit. For this detector system, the fitted parameters were: a=271, b=254, d=-490 and e=0.52. The function for $\varepsilon(662\ keV, \theta)$ can then be substituted into equation 1 to calculate count rates from ^{137}Cs sources.

There are two common orientations for a detector in a backpack. In one, the crystal is at the bottom (θ=0 downwards) and in the other the crystal is at the top (θ=0 upwards). The choice of orientation will depend on survey requirements. The detector down option will result in the detector being closer to the ground, and maximise sensitivity to radiation originating within a small solid angle below the detector. The detector up option increases the detector height and widens the field of view with a greater contribution for radiation from wider angles. The detector up option sacrifices some spatial resolution for area coverage and may be preferred for larger area surveys of dispersed activity. The detector down option sacrifices some area coverage for increased spatial resolution and sensitivity to close objects. It may be preferred for smaller area surveys with highly localised activity distribution, such as source searches. In this work, measurements and modelling were conducted for the detector up configuration.

2.4 Numerical Model

The basis of the numerical model used **Eq. 1,** to calculate the number of counts reaching a detector at height h above the ground for a source of activity A_s at depth D below the ground surface. The system geometry is shown in Figure 2. Realistically when the backpacks are

worn they are held slightly out from the operator's back. To take account of the detector radius, dimensions of thermal insulation in the housing, and the effects of the detector frame, the numerical model includes an offset distance *d*.

The path lengths through the soil, air and the operator vary with both polar and azimuthal angles (θ and φ) and are calculated using simple trigonometry for the cuboid substitute operator shape. These are given by:

$$P_{body} = \frac{L/2}{\cos\varphi \sin\theta} - \frac{d}{\sin\varphi \sin\theta} \quad \text{where } \varphi_{min} < \varphi < \varphi_c$$

$$P_{body} = \frac{d+W}{\sin\varphi \sin\theta} - \frac{d}{\sin\varphi \sin\theta} = \frac{W}{\sin\varphi \sin\theta} \quad \text{where } \varphi > \varphi_c$$

$$P_{body} = 0 \quad \text{where } \varphi < \varphi_{min}$$

$$P_{soil} = D/\cos\theta$$

$$P_{air} = P_{total} - P_{body} - P_{soil}$$

For critical azimuthal angles φ_{min} and φ_c for the minimum angle where the gamma ray passes through the operator and the angle where the gamma ray passes through the corner of the operator.

$$\tan\varphi_{min} = 2d/L$$

$$\tan\varphi_c = 2(d+W)/L$$

Corresponding critical polar angles, θ_{max} and θ_c, and path length are defined for radiation originating from the area underneath the operator. This accounts for less than 1% of the detector field of view, and is not considered a significant factor in the model results. These angles and path lengths are included in supplementary material for completeness.

The mass attenuation coefficients have been calculated and the angular efficiency measured. The activity of the source and the detector area are also known values. Therefore the model can predict the count rate reaching the detector from the source at any position.

Two versions of the numerical model were implemented. The first simulated the experimental configuration (described below, Section 2.5). The second simulated a laterally

uniform source over a larger area, using a regular grid of points at 0.1 m spacing over a 10x10 m area. The benefit of the numerical model is that variables can be easily changed, the offset distance *d* was increased to test any changes in the measured count rate, and also the source depth can be varied.

2.5 Experimental Set Up and Method

For the experiment a ^{137}Cs point source of activity 250 kBq was used. To approximate a uniform field a hexadecagon was mapped out around a fixed centre-point. The backpack detector was suspended from a metal frame 90 cm above the centre-point, supported within the inside edge of the hexadecagon grid. Distances of 1.0 m, 1.5 m and 2.5 m were marked along each of the 16 radii. The ^{137}Cs source was placed at different positions for periods of time calculated to approximate a uniform distribution, determined by the area each position mapped out, illustrated in Figure 3. The corresponding areas and the times for each source position in a single sequence of measurements are given in Table 5.

Each sequence of measurements consisted of background measurements recorded without the source, followed by measurements using the ^{137}Cs source. The sequence was completed within half an hour, minimising the potential effects of thermal drift in the detector. These were repeated with the substitute operator, an array of plastic rectangular boxes 30x40 cm stacked to a combined height of 116 cm and filled with water.

3. Results

3.1 Results of the Experimental Model

Net spectra for measurements with and without the substitute operator are shown in Figure 4. There is clear difference in the intensity of the ^{137}Cs full-energy peak. Counts rates for the ^{137}Cs peak (600-720 keV) without the substitute operator were 6.2 ± 0.1 s^{-1}, and 4.9 ± 0.1 s^{-1} with the operator present. The substitute operator thus reduces full-energy detection efficiency by 21.1 ± 3.0%.

Comparisons can also be made between the background spectra recorded with and without the substitute operator present. Measurements of the background with human operators can then be used to compare the substitute operator to humans. A direct validation of the observed reduction factors in the point source experiment was not undertaken as exposing human operators to radiation from point sources in excess of the environmental dose rate was not considered to be ethical.

The results of these measurements at SUERC, where the background is due to natural sources, for count rates in the 450-3000 keV spectral window, are given in Table 6 for the water filled containers and two operators with heights and weights comparable to the ICRU89 reference adults. These show that for dose rates dominated by natural activity the operator effect across the whole spectrum is lower than that observed at 662 keV for ^{137}Cs sources. The substitute operator comprising water filled plastic containers produces a reduction in total count rate that is in agreement with that measured for operator A, whereas operator B had a similar, but slightly smaller effect on the total count rate.

3.2 Results of the Numerical Model

As stated above the numerical model has been applied to the measured geometry and tabulated linear attenuation parameters for 662 keV gamma energy, corresponding to the full-energy peak of ^{137}Cs. The model of the experimental system predicts a reduction in count rate due to the operator of 23.6%. The model of sources on a larger, regular grid (as described in section 2.4), predicted an operator effect of 26.1%. This is a slightly larger reduction in ^{137}Cs peak count rate although of similar magnitude. In both cases the estimated values correspond to detector offset positions of 0.13 m. The second analysis, with a larger number of source positions presents a slightly different geometry than the first simulation. In particular it includes the influence of a larger proportion of gamma rays incident at shallow angles from distances beyond the 2.5 m outer ring of the experiment, and sources at positions directly under the substitute operator. These difference between the two model estimates is therefore attributed to these geometrical effects. The model results are broadly in agreement with the observed values using a substitute operator, although it is noted that slightly larger reductions in ^{137}Cs peak count rate were predicted than those observed in the experiment. Experimental factors including difficulty completely filling the containers with water, and accounting for

interfaces between containers may be partially responsible for the small differences, as would shape dependent differences between simulated and real operators.

The model can also be used to evaluate the operator effect under different conditions. The effect of changing the operator-detector separation, *d*, and the effect of increased source burial depth have been examined. The models used a detector height of 0.9 m, which was limited by the frame height in the experiment. In practice, the detector is carried at a height of approximately 1.2 m. Table 7 shows the reduction in ^{137}Cs peak count rate for different model conditions. As expected the detector offset position has a marked influence on operator attenuation factors. Whereas a 20% reduction is expected for a detector set 20 cm from the operator, this rises inversely with offset distance – with some 34% reduction for a detector held 6 cm from the back of the substitute operator. For subsurface activity, increased burial depth reduces the field of view of the detector, increasing the proportion of radiation passing through the length of the operator and hence increasing the reduction in peak count rate due to the operator. The detector height has a negligible effect.

3.4 Results of the Field Validation

Measurements with and without human operators in radiation fields dominated by ^{137}Cs and ^{134}Cs were conducted at a ground sampled calibration site at Fukushima University (Sanderson et al. 2013). These measurements are shown in Figure 5, and give reductions in the full energy intensities for ^{134}Cs and ^{137}Cs of 25-30%, which are consistent with the results of the numerical model developed in this study, and with the experimental values obtained from the substitute experimental geometry. Comparisons between measurements with the backpack system and data from soil samples at the ECCOMAGS calibration sites (Sanderson et al 2004) close to the Solway Firth in Scotland (Cresswell et al. 2013) have also shown reductions of 20% to 40% between the field measurements and samples. The magnitude of the observed reductions is compatible with the estimate from the model presented here.

4. Discussion and Conclusion

Radiometric measurements surveying a radiation field in the environment are complex. The results are not only influenced by the geometrical distribution and types of radioisotopes and the geometrical distribution and material composition of passive materials in the environment, but crucially by the detector response function and the materials surrounding the detector. An example of this is the impact of a human operator on the spectral shape and intensities in backpack surveys.

This effect has been investigated using a combination of experimental and numerical modelling, with comparison to field measurements. A simplified experiment using a water filled cuboid was carried out to investigate this effect experimentally and in comparison with a numerical model based on tabulated linear attenuation coefficients. The experiment measured an overall reduction ^{137}Cs peak count rate of 21 ± 3.0%. The numerical model of the same set up calculated reductions of 23-26%, confirming that attenuation factors of this magnitude are to be expected, and must be taken account of in system calibration. The results of the experimental and numerical models are consistent with field measurements at Fukushima University and the ECCOMAGS calibration sites on the Solway Firth, Scotland.

The reduction in count rate in the 450-3000 keV window, which can be scaled directly to dose rate, for natural radiation fields, ~15%, was significantly less than that observed for the ^{137}Cs full energy peak and for radiocaesium dominated radiation fields at Fukushima University. The attenuation of higher energy gamma rays present from natural sources would be less than that for radiocaesium. In addition, partial energy absorption within the operator would lead to an increase in scattered gamma rays interacting with the detector resulting in a compensatory increase in count rate at lower energy. The numerical model used here examines full energy deposition and does not address the impact of the operator on scattered radiation.

The offset distance between the back of the human operator and the centre of the detector was identified as crucial parameter influencing the observed reduction. An increase from 0.13 to 0.20 m in the numerical model changed the reduction in count rate from 26.1% to 20.1%, suggesting that the influence of the human operator can be reduced by increasing the distance of the detector from the operators back. Increasing the burial depth of the activity results in a small increase in the operator effect.

Measurements of the operator effect on ambient natural radiation fields show that the substitute operator is comparable to human operators, with some variation between operators that could warrant further quantification. Data were collected with two operators, with height and weight similar to the reference adults described in ICRU89. The reduction in measured total count rate for the female operator was less than for the male operator. The male and female body shape differs as does the weight distribution, men tending to have broader shoulders and waists which are the parts of the body closest to the detector and hence expected to have the largest impact on the attenuation of the measured radiation.

The operator introduces directionality to the system response by significantly reducing the detection efficiency for radiation originating in front of the operator. Mapping the angular response of the detector with the operator generates information that may be of considerable benefit in evaluating radiometric data, especially from highly heterogeneous environments. In some situations, for example source searches on beaches, it may be beneficial for the operator to carry the detector in front. This would maximise signals from any sources in front of the operator, increasing the opportunity to identify and locate it before potentially disturbing the source by walking over it.

The observed effect is not particular to the use of a backpack system, but will be present for any radiation detection system studying a complex source distribution operated in close vicinity to the human body, or other attenuating structures such as vehicle components. Common practice for dose rate measurements with the probe held at a fixed height away from the body will experience a significantly smaller effect than observed in this study. However, unlike the backpack system where the operator and detector are in a fixed geometry hand held detector systems may be used in situations where the position relative to the operator is not fixed, with corresponding variability in operator attenuation. Again, the position of the operator may be a factor where radioactive material is distributed heterogeneously. Detector systems mounted on vehicles may experience significant attenuation from the engine, or other substantial components, and proximity to a fuel tank would provide a time-varying attenuation factor (Malins et.al. 2015). Care may also be needed in relating measurements with integrating personal dosimeters worn close to the body, or similar instruments increasingly being fitted on collars for dosimetric studies of wildlife (Hinton et.al. 2015), with environmental dose rates.

References

Aage, H.K., Korsbech, U., 2003. Search for lost or orphan radioactive sources based on NaI gamma spectrometry. Applied Radiation and Isotopes**,** 58, 103–113. doi:10.1016/S0969-8043(02)00222-1

Bucher, B., Rybach, L., Schwarz, G., 2008. Search for long-term radiation trends in the environs of Swiss nuclear power plants. Journal of Environmental Radioactivity, 99**,** 1311–1318. doi:10.1016/j.jenvrad.2008.04.004

Cresswell, A.J., Sanderson, D.C.W., 2012. Evaluating airborne and ground based gamma spectrometry methods for detecting particulate radioactivity in the environment: A case study of Irish Sea beaches. Science of the Total Environment, 437, 285–296. http://dx.doi.org/10.1016/j.scitotenv.2012.08.064

Cresswell, A.J., Sanderson, D.C.W., Harrold, M., Kirley, B., Mitchell, C., Weir, A., 2013. Demonstration of lightweight gamma spectrometry systems in urban environments. Journal of Environmental Radioactivity, 124, 22-28. http://dx.doi.org/10.1016/j.jenvrad.2013.03.006

Drovnikov, V.V., Egorov, N.Y., Kovalenko, V.V., Serboulov, Y.A., Zadorozhny, Y.A., 1997. Some results of the airborne high energy resolution gamma-spectrometry application for the research of the USSR European territory radioactive contamination in 1986 caused by the Chernobyl accident. Journal of Environmental Radioactivity, 37, 223-234. doi:10.1016/S0265-931X(96)00093-8

Giles, J. R., Roybal, L. G., Carpenter, M. V., Oertel, C. P., Jacobson, J. J., Eaton, D. L., Schwendiman, G. L., 2005. Real-time remediation utilizing the backpack sodium iodide system and the U.S. EPA Triad approach. In: Waste Management 2006 Conference, February 26-March 2, 2006, Tucson, AZ. INL/CON-05-00373.

Hinton, T.G., Byrne, M.E., Webster, S., Beasley, J.C., 2015. Quantifying the spatial and temporal variation in dose from external exposure to radiation: a new tool for use on free-ranging wildlife. Journal of Environmental Radioactivity, 145, 58-65. doi: 10.1016/j.jenvread.2015.03.027

Hjerpe, T., Samuelsson, C., 2006. Shielded and unshielded geometries in the search for orphan sources. Applied Radiation and Isotopes, 64, 551–555. doi:10.1016/j.apradiso.2005.11.017

Hubbell, J.H., Seltzer, S.M., 2004. Tables of X-Ray Mass Attenuation Coefficients and Mass Energy-Absorption Coefficients (version 1.4). National Institute of Standards and Technology, Gaithersburg, MD. Available at: http://physics.nist.gov/xaamdi.

International Atomic Energy Agency, 1991. Airborne Gamma Ray Spectrometer Surveying. IAEA, Vienna. Technical Reports Series 323.

International Atomic Energy Agency, 2003. Guidelines for Radioelement Mapping Using Gamma Ray Spectrometry Data. IAEA, Vienna. IAEA-TECDOC-1363.

International Commission on Radiological Protection, 1975. The Report of the Group Task on Reference Man. ICRP Publication 23.

International Commission on Radiological Protection, 2002. Basic Anatomical and Physiological Data for Use in Radiological Protection: Reference Values. ICRP Publication 89.

Kobayashi, S., Shinomiya, T., Kitamura, H., Ishikawa, T., Imaseki, H., Oikawa, M., Kodaira, S., Miyaushiro, N., Takashima, Y., Uchihori, Y., 2015. Radioactive contamination mapping of northeastern and eastern Japan by a car-borne survey system, Radi-Probe. Journal of Environmental Radioactivity, 139, 281-293. http://dx.doi.org/10.1016/j.jenvrad.2014.07.026

Kock, P, Rääf, C, Samuelsson, C., 2014. On background radiation gradients - the use of airborne surveys when searching for orphan sources using mobile gamma-ray spectrometry. Journal of Environmental Radioactivity, 128, 84-90. http://dx.doi.org/10.1016/j.jenvrad.2013.10.022

Long, S., Martin, L., 2007. Optimisation of systems to locate discrete gamma-ray sources within a large search area. Journal of Environmental Radioactivity**,** 94, 41-53. doi:10.1016/j.jenvrad.2006.12.012

Lyons, C., Colton, D., 2012. Aerial measuring system in Japan. Health Physics, 102, 509-515. DOI: 10.1097/HP.0b013e31824d0056

Malins, A., Okumura, M., Machida, M., Takemiya, H., Saito, K., 2015. Fields of View for Environmental Radioactivity, in: Takahashi, T., Yamana, H., Tsukada, H., Sato, N., Nakatani, M, (Eds.), Proceeding of the International Symposium on Radiological Issues for Fukushima's Revitalized Future. pp. 28-34. Office of KUR Research Program for Scientific Basis of Nuclear Safety, Kyoto University Research Reactor Institute. ISBN-978-4-9906815-3-1 (Book) C3053, ISBN-978-4-9906815-4-8 (CD) C3853, ISBN-978-4-9906815-5-5 (from Web) C3853.

Mellander, H., 1989. Airborne gamma spectrometric measurements of the fallout over Sweden after the nuclear reactor accident at Chernobyl, USSR. IAEA/NENF/NM-89-1.

Minty, B.R.S., 2011. Airborne geophysical mapping of the Australian continent. Geophysics, 76, A27-A30.

Nilsson, J.M.C., Östlund, K., Söderberg, J., Mattsson, S., Rääf, C., 2014. Tests of HPGe- and scintillation-based backpack γ-radiation survey systems. Journal of Environmental Radioactivity, 135, 54-62. http://dx.doi.org/10.1016/j.jenvrad.2014.03.013

Sanada, Y., Sugita, T., Nishizawa, Y., Kondo, A., Torii, T., 2014. The aerial radiation monitoring in Japan after the Fukushima Daiichi nuclear power plant accident. Progress in Nuclear Science and Technology, 4, 76-80. DOI: 10.15669/pnst.4.76

Sanderson, D.C.W, Scott, E.M., 1989. Aerial Radiometric Survey in West Cumbria in 1988. MAFF Report N611. Available at: http://eprints.gla.ac.uk/57332/

Sanderson, D.C.W, East, B.W., Scott, E.M., 1989. Aerial Radiometric Survey of Parts of North Wales in July 1989. SURRC Report. Available at: http://eprints.gla.ac.uk/57596/

Sanderson, D. C. W., Allyson, J. D., Cairns, K.J., MacDonald, P.A., 1990a. A Brief Aerial Survey in the Vicinity of Sellafield in September 1990. SURRC Report. Available at: http://eprints.gla.ac.uk/57750/

Sanderson, D. C. W., Allyson, J. D., Martin, E., Tyler, A. N., Scott, E.M. 1990b. An Airborne Gamma ray Survey of Three Ayrshire Districts. SURRC Report for the district councils of Cunninghame, Kilmarnock & Loudoun, and Kyle & Carrick. Available at: http://eprints.gla.ac.uk/57634/

Sanderson, D. C. W., Allyson, J. D., Tyler, A. N., 1992a. An Aerial Gamma Ray Survey of Chapelcross and its Surroundings in February 1992. SURRC Report for British Nuclear Fuels plc. Available at: http://eprints.gla.ac.uk/58260/

Sanderson, D. C. W., Allyson, J. D., Tyler, A. N., Murphy, S., 1992b. An Aerial Gamma Ray Survey of Springfields and the Ribble Estuary in September 1992. SURRC Report for British Nuclear Fuels plc. Available at: http://eprints.gla.ac.uk/57327/

Sanderson, D. C. W., Allyson, J. D., Tyler, A. N., Ni Riain, S., Murphy, S., 1993a. An Airborne Gamma Ray Survey of Parts of SW Scotland in February 1993. Final Report. SURRC Report for the Scottish Office Environment Department (HMIPI). Available at: http://eprints.gla.ac.uk/59483/

Sanderson, D. C. W., Scott, E.M., Baxter, M.S., Martin, E., Ni Riain, S., 1993b. The Use of Aerial Radiometrics for Epidemiological Studies of Leukaemia: a Preliminary Investigation in SW England. SURRC Report for the Leukaemia Research Fund. Available at: http://eprints.gla.ac.uk/57742/

Sanderson, D. C. W., Allyson, J. D., Tyler, A. N., 1994a. Rapid quantification and mapping of radiometric data for anthropogenic and technically enhanced natural nuclides. In: Application of Uranium Exploration Data and Techniques in Environmental Studies. IAEA, Vienna. pp 197-216. IAEA TECDOC-827.

Sanderson, D. C. W., Allyson, J. D., Tyler, A. N., Scott, E. M., 1994b. Environmental applications of airborne gamma spectrometry. In: Application of uranium exploration data and techniques in environmental studies. IAEA, Vienna. pp 71-91. IAEA TECDOC-827.

Sanderson, D.C.W., Allyson, J.D., Ni Riain, S., Gordon, G., Murphy, S., Fisk, S., 1994c. An Aerial Gamma Ray Survey of Torness Nuclear Power Station on 27th-30th March 1994. SURRC Report for Scottish Nuclear Limited. Available at: http://eprints.gla.ac.uk/58355/

Sanderson, D.C.W., Allyson, J.D., Gordon, G., Murphy, S., Tyler, A. N., Fisk, S., 1994d. An Aerial Gamma Ray Survey of Hunterston Nuclear Power Station in 14-15 April and 4 May 1994. SURRC Report for Scottish Nuclear Limited. Available at: http://eprints.gla.ac.uk/39213/

Sanderson, D.C.W., Ferguson, J.M., 1997. The European capability for environmental airborne gamma ray spectrometry. Radiation Protection Dosimetry, 73, 213-218.

Sanderson, D.C.W., Cresswell, A.J., Scott, E.M., Lang, J.J., 2004. Demonstrating the European Capability for Airborne Gamma Spectrometry: results from the ECCOMAGS Exercise. Radiation Protection Dosimetry, 109, 119-125. DOI: 10.1093/rpd/nch243

Sanderson, D.C.W., Cresswell, A.J., Seitz, B., Yamaguchi, K., Takase, T., Kawatsu, K., Suzuki, C., Sasaki, M., 2013. Validated Radiometric Mapping in 2012 of Areas in Japan Affected by the Fukushima-Daiichi Nuclear Accident. Glasgow:University of Glasgow. ISBN 978-0-85261-937-7. Available at: http://eprints.gla.ac.uk/86365/

Storm, E., Israel, H. I., 1970. Photon cross sections from 1 keV to 100 MeV for elements Z = l-100. Nuclear Data Tables, A 7, 565-681.

Tanigaki, M., Okumura, R., Takamiya, K., Sato, N., Yoshino, H., Yamana, H., 2013. Development of a car-borne γ-ray survey system, KURAMA. Nuclear Instruments and Methods in Physics Research, A726, 162-168. http://dx.doi.org/10.1016/j.nima.2013.05.059

Tsuda, S., Yoshida, T., Tsutsumi, M., Saito, K., 2015. Characteristics and verification of a car-borne survey system for dose rates in air: KURAMA-II. Journal of Environmental Radioactivity, 139, 260-265. http://dx.doi.org/10.1016/j.jenvrad.2014.02.028

Tyler, A.N., Heal, K.V., 2000. Predicting areas of ^{137}Cs loss and accumulation in upland catchments. Water, Air, and Soil Pollution, 121, 271–288.

Winkelmann, I., Strobl, C., Thomas, M., 2004. Aerial measurements of artificial radionuclides in Germany in case of a nuclear accident. Journal of Environmental Radioactivity**,** 72, 225-231. doi:10.1016/S0265-931X(03)00205-4

Table 1 Physical characteristics for reference adults taken from ICRP (1975, 2002).

	ICRP23 (1975)		ICRP89 (2002)	
	Male	Female	Male	Female
Mass (kg)	70	58	73	60
Height (m)	1.70	1.60	1.76	1.63
Density (kg m^{-3})	1070	1040		

Table 2 The major chemical element composition of the human body with corresponding percentage per mass of the 70 kg reference man (ICRP 1975).

Element	Mass of element in 70kg Person (kg)	Percent by Mass (%)
Oxygen (O)	43	61.35
Carbon (C)	16	22.82
Hydrogen (H)	7	9.99
Nitrogen (N)	1.8	2.57
Calcium (Ca)	1	1.43
Phosphorus (P)	0.78	1.11
Minor elements	0.51	0.73

Table 3 Human Body Mass Attenuation Coefficients derived from the material composition and the elemental mass attenuation coefficients. The linear attenuation coefficient is obtained by using the average body density, neglecting anatomical variations. Values for ^{137}Cs (662 keV) were determined by interpolation between tabulated values.

Energy (keV)	Mass Attenuation Coefficient ($m^2\,kg^{-1}$)	Linear Attenuation Coefficient (m^{-1})
30	0.052796	56.0691
40	0.032341	34.34655
50	0.024746	26.2803
60	0.021087	22.39471
80	0.017673	18.76885
100	0.016008	17.00037
150	0.013812	14.6686
200	0.012481	13.25447
300	0.010778	11.44662
400	0.009633	10.2306
500	0.008775	9.318863
600	0.008118	8.621373
662	*0.00782*	*8.3048*
800	0.00713	7.571909
1000	0.006408	6.805753
1500	0.005203	5.525981

2000	0.004475	4.752764
3000	0.003614	3.838343
4000	0.003124	3.317709
5000	0.002801	2.974734
6000	0.002574	2.733089

Table 4 The comparison of water and PVC plastic as a substitute material for the human body for 662 keV, with other media that gamma rays are likely to travel through in the environment of the experiment.

Medium	Density (kg/m^3)	Mass Attenuation (m^2/kg)	Linear Attenuation (m^{-1})
Water	1000	0.00874	8.7400
Plastic (PVC)	1300	0.00808	10.5040
Air	1.225	0.00775	0.0095
Soil	1400	0.00769	10.7660

Table 5 Time that the gamma ray source was placed at a corresponding radial distances.

Segment	Area (m^2)	Time (s)
A1	1.00	30.0
A2	0.49	14.7
A3	0.26	7.8
A4	0.0.5	1.5

Table 6 Human operator reduction in natural background environment.

Operator	Weight (kg)	Height (cm)	Gender	Reduction (%)
Substitute				15.2 ± 0.5
A	75	175	Male	15.8 ± 1.0
B	61	160	Female	13.6 ± 1.1

Table 7 Reductions in ^{137}Cs peak count rates due to the operator determined by the numerical model for different detector-operator offset distances, *d*, and source depth *D*.

Depth (m)	Offset (m)	Height (m)	Reduction (%)
0	0.06	0.9	34.1
0	0.13	0.9	26.1
0	0.13	1.2	26.4
0	0.20	0.9	20.1
0.01	0.13	0.9	26.5
0.05	0.13	0.9	27.9
0.10	0.13	0.9	28.7
0.10	0.13	1.2	28.9

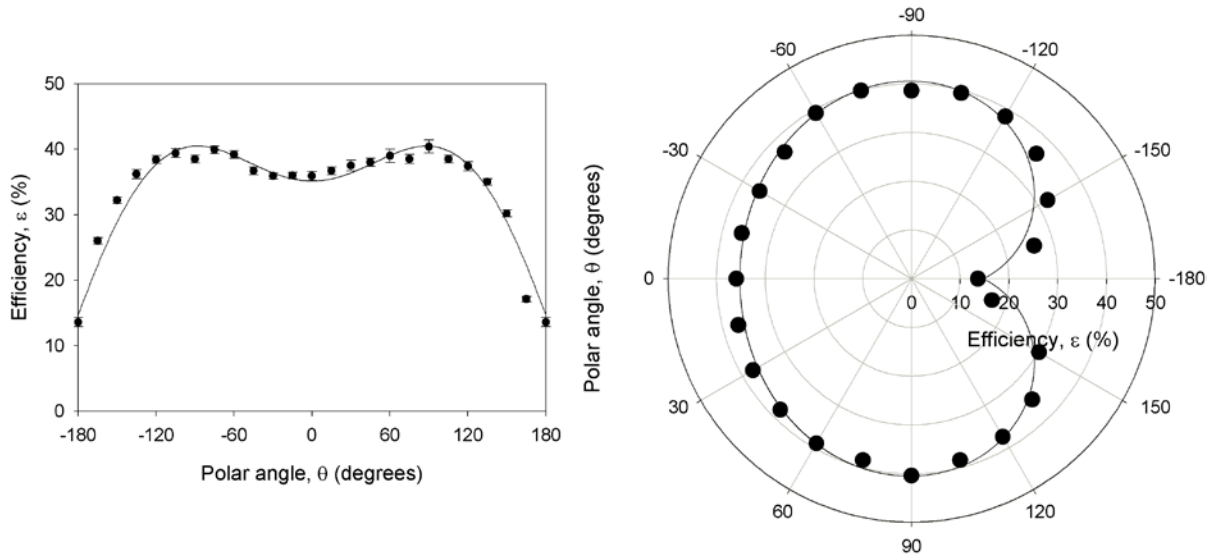

Figure 1: Angular dependence of the efficiency for the SUERC backpack system.

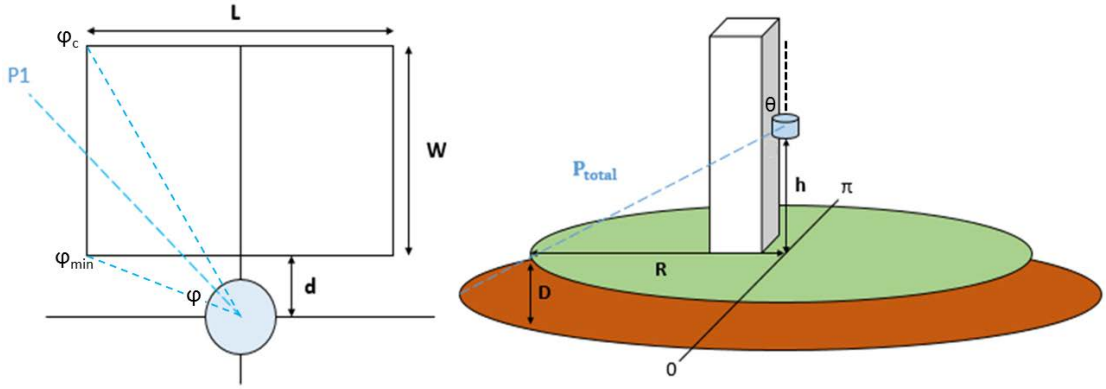

Figure 2: Geometry of the numerical model, showing a detector at height *h* above the ground with an operator with a simplified cuboid geometry with width *L*, depth *W* and a detector-operator offset of *d*. The source is at distance *R*, azimuthal angle φ and depth *D* below the ground surface.

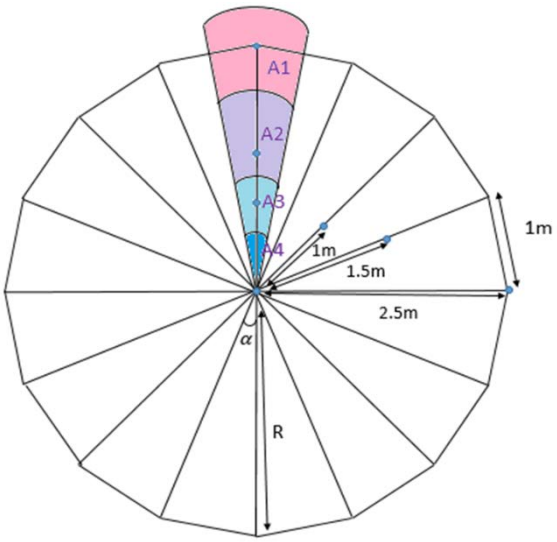

Figure 3: Hexadecagon grid marked to create uniform field. Positions *R*, angle α and segment areas *A* used to calculate period of time source must be placed at each position to create a uniform field.

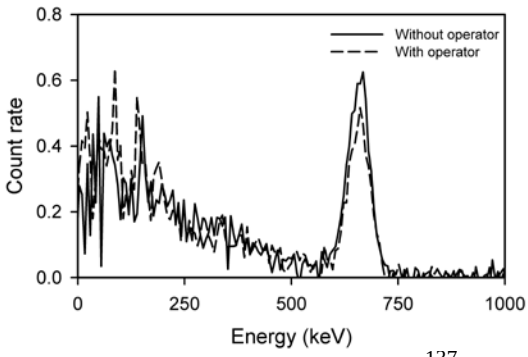

Figure 4: Gamma ray spectra for ^{137}Cs, with and without substitute operator present. The reduction in the full energy peak count rate when the operator is shielding the detector is 21.1±3.0%.

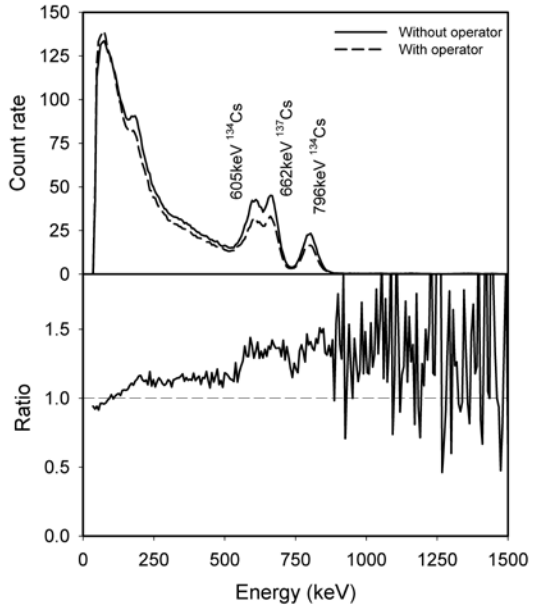

Figure 5: Measurements conducted near the calibration site at Fukushima University, 4th November 2012, with and without the operator present. With the recorded spectra (top) and the ratio of count rates without the operator to those with the operator present (bottom).